

# **Through-Linker Intramolecular Singlet Fission: General Mechanism and Designing Small Chromophores**

Tao Zeng\*

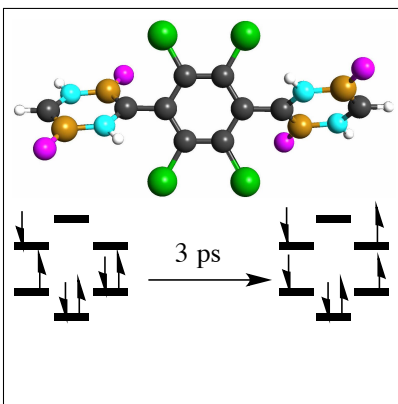
*Department of Chemistry, Carleton University, Ottawa, Ontario, K1S5B6, Canada*

E-mail: [toby.zeng@carleton.ca](mailto:toby.zeng@carleton.ca)

## Abstract

We perform quantum chemistry calculations and quantum dynamics simulations to investigate covalent linker's through-bond effects in intramolecular singlet fission. A model molecule with two diazadiborine chromophore units and the *para*-phenylene linker is proposed. A general, step-by-step picture for the conversion from the single- to the multi-excitonic state through the linker is presented. Based on the picture, we discuss the triplet-pair delocalization into the linker and design two more chromophores with higher fission efficiency. All three designed chromophores have promising ps fission time scales and make good candidates for azaborine synthesis.

## Graphical TOC Entry



## Keywords

Singlet Fission; Non-Adiabatic Dynamics; Multireference Perturbation Theory; Multi-Configurational Time-Dependent Hartree; Azaborine Chemistry

Singlet fission (SF) is a fascinating process that splits a singlet exciton, generated upon absorbing one photon, to two triplet excitons.<sup>1,2</sup> With the one photon to two excitons number doubling and the longer lifetime of the triplet excitons, it can raise the energy conversion efficiency of single-junction photovoltaic devices to surpass the  $\sim 33\%$  Shockley-Queisser limit.<sup>3</sup> This efficiency enhancement is critical for the development of the third generation solar cells.<sup>4</sup> SF starts with a spin-conserved step that converts the singlet exciton to a singlet spin-coupled state of two triplets, which subsequently undergoes spin-disentanglement and exciton diffusion to give two independent triplets. The SF efficiency is highly sensitive to the inter-chromophore configuration.<sup>5-8</sup> The difficulty in engineering the molecular packing morphology motivated the idea of intramolecular singlet fission (iSF):<sup>9-12</sup> to have the fission occur within one molecule that connects multiple chromophore units and adjust their configuration through the more controllable covalent bonding and intramolecular steric hindrance. After years of endeavour, promising iSF quantum yield had been achieved since 2015.<sup>13-18</sup>

The advance in the field of SF is limited by the paucity of capable chromophores.<sup>11,19</sup> An SF-capable material should have its chromophore unit satisfy  $E(S_1) \geq 2E(T_1)$ ,  $S_1$  and  $T_1$  being the lowest singlet and triplet excited states, so that the  $S_1 \rightarrow 2T_1$  fission is thermodynamically favorable. This requirement narrows the pool of candidates as they need to possess weak/intermediate diradical character in ground state.<sup>20</sup> Chromophore units satisfying this requirement have mainly tetraradical (triple-pair) character in the lowest singlet excited state ( $S_1^d$ ) of their dimer (denoted by “ $d$ ”). The triplets are bound through mixing-in charge-transfer character,<sup>21</sup> which lowers the  $S_1^d$  energy. The binding strength is proportional to the energy gap between  $S_1^d$  and the lowest quintet state ( $Q_1^d$ ) of pure tetraradical character.<sup>22</sup> The spin-disentanglement is induced by the spin dipole-dipole (SDD) interaction of  $\sim 0.1 \text{ cm}^{-1}$  magnitude that only couples  $S_1^d$  and  $Q_1^d$  given a small gap between them.<sup>1</sup> The small gap is the second requirement for SF chromophores.  $T_3^d$  is also of triplet-pair character but not SDD-coupled to  $S_1^d$  due to the symmetry of the molecules in this work.

To break through the paucity constraint, people have been trying to design SF-chromophores

using computational chemistry. 1,3-diphenylisobenzofuran is a typical successful case.<sup>23,24</sup> A recently surging motif is to design chromophores of small size<sup>25-29</sup> for their following benefits: (1) they are computationally friendly and support high level theoretical studies. They hence serve as models to investigate SF mechanism; (2) for stable small chromophores, their use leads to high exciton density and facilitates the fabrication of mini photovoltaic devices; (3) small models that are not chemically persistent can serve as structural cores to derive larger yet realistic chromophores, just like  $\text{CH}_2$  vs persistent carbenes. The first purpose of this letter is to present our designed small iSF chromophores with a covalent linker. As recently shown by Sanders et al.,<sup>16,30</sup> introducing a linker between chromophore units, especially when the fission occurs solely through the linker (i.e., in the absence of through-space or through-contact iSF), can prevent rapid recombination of the triplet-pair. Despite its importance, the mechanism of how a linker participates in iSF is unclear. Therefore, the second, more important objective is to use the designed chromophores as models to extract a general, step-by-step through-linker iSF picture. This picture guides us to make substitutions on the phenylene to enhance iSF efficiency.

Computational details are given in Section S1 in the supporting information (SI). In brief, we use density functional theory method with the M06-2X functional<sup>31</sup> to optimize the ground state structures of all molecules considered. Coordinates of all discussed structures are given in Section S6. Excited state electronic structure calculations are carried out using the general multi-configurational quasi-degenerate perturbation theory (GMC-QDPT)<sup>32</sup> with a 6 electrons in 6 orbitals active space that include the HOMO and LUMO of the two chromophore units and the linker (Figure 1). The linear vibronic coupling Hamiltonians are prepared using a model space diabaticization scheme<sup>33</sup> adapted<sup>34</sup> to GMC-QDPT wave functions. The cc-pVDZ basis set<sup>35</sup> is used except for Cl atom, which is described using the double-zeta model core potential basis set.<sup>36</sup> All electronic structure calculations are performed using GAMESS-US.<sup>37,38</sup> The iSF dynamics is simulated using the multi-configurational time-dependent Hartree (MCTDH) method.<sup>39</sup>

We choose the 2,5-difluoro-1,4-diaza-2,5-diborine **1** (Figure 1) designed molecule<sup>26</sup> as the chromophore unit to construct the iSF chromophore. **1** can be viewed as consisting of two BN-substituted methyl radicals, which bring about its diradical character. The F atoms further enhance this character to have  $E(S_1) > 2E(T_1)$ .<sup>26</sup> Our purpose of choosing the **1**-unit is to cross-link SF with the vibrant field of azaborine chemistry.<sup>40,41</sup> The synthesis of **1** or structures based on this core has not been reported. However, the chemically persistent **2** and **2'** that share similar structural features with **1** have been synthesized.<sup>42,43</sup> This raises our confidence on the future synthesis of the designed chromophores here. The *para*-phenylene is chosen to be the linker. It spatially separates the chromophore units so that we can isolate the through-linker effects from the through-space/through-contact effects.

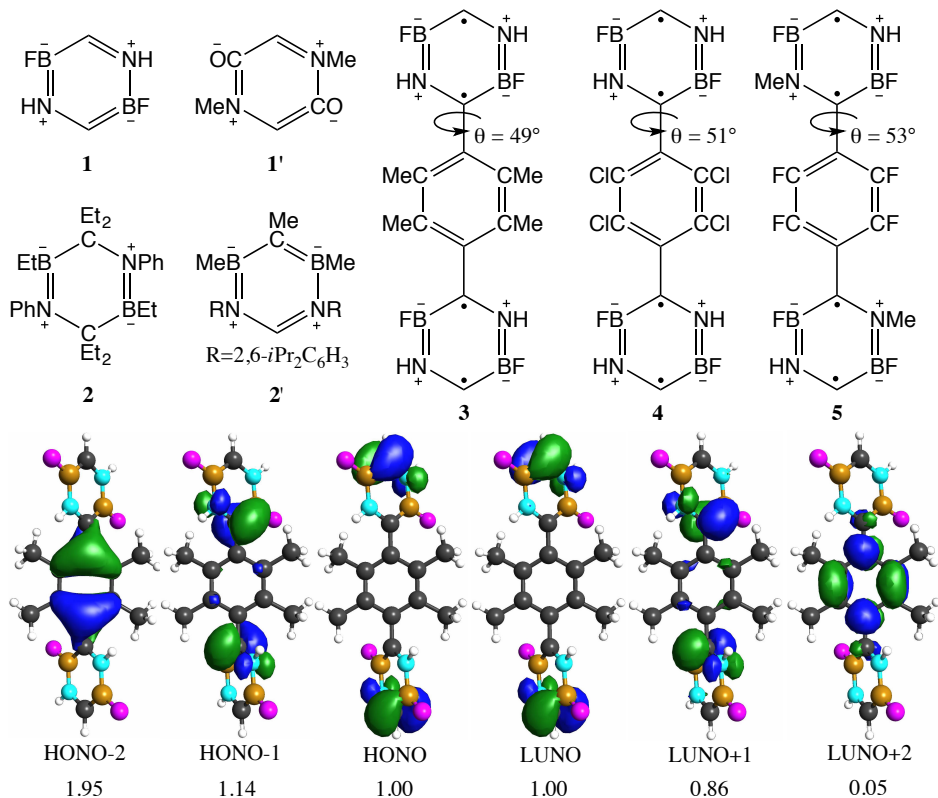


Figure 1: All structures (**1–5**) discussed in the letter and the natural orbitals of **3** in the 606e active space.  $\theta$  is the dihedral angle between the chromophore unit and the linker. The  $\theta$  values and Lewis structures are given for **3–5** at their  $S_1^d$  state. In the orbital panels, H, B, C, N, and F atoms are represented by white, brown, black, cyan, and purple spheres. The blue and green lobes represent the orbitals. HONO and LUNO stand for highest occupied and lowest unoccupied natural orbitals.<sup>20</sup> The occupation numbers are given under the orbitals.

The first designed chromophore **3** (**4** and **5** below too) is of  $C_2$  symmetry with the  $C_2$  axis perpendicular to the linker’s plane. Four methyls are introduced to the linker to enlarge the **1**-linker dihedral angles ( $\theta$ ). This is to reduce the **1**-linker  $\pi$ -interaction, which significantly lowers the  $S_1^d$  energy and gives a 0.66 eV large  $S_1^d$ - $Q_1^d$  gap when without the methyls. The methyls increase  $\theta$  from 12 to 49° in **3**’s  $S_1^d$  structure and its 0.86 LUNO+1 occupancy (Figure 1) indicates 86% tetraradical character.<sup>20</sup> Accordingly, the minimum-to-minimum  $S_1^d$ - $Q_1^d$  gap is reduced to 0.08 eV. The spin-conserved step of SF starts with the lowest bright singlet excited state at vertical excitation and end with  $S_1^d$  at its optimized structure. The energy difference between the two states (called “iSF exoergicity” below) is evaluated to be 0.48 eV, much larger than the 0.08 eV gap. Therefore, the vibrational energy released in the iSF can easily fill the gap and lead to (pseudo-)degeneracy of the  $S_1^d$  and  $Q_1^d$  vibronic levels, facilitating the spin-disentanglement.

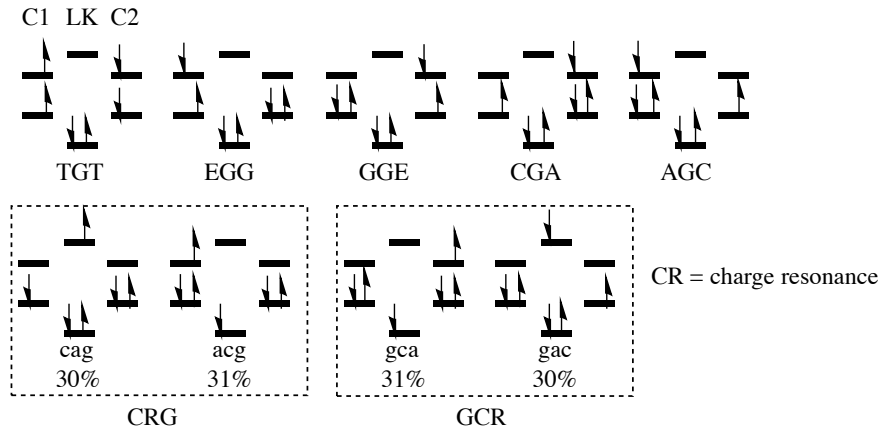


Figure 2: Leading configurations of the seven most relevant diabats for the iSF in **3**. The occupation schemes of the HOMO (lower horizontal bar) and LUMO (higher) of each fragment are presented. The vertical arrows denote spins-up and -down. Each of the *CRG* and *GCR* diabats contain two leading configurations in the corresponding dashed boxes.

A fast singlet fission requires sufficient coupling between the single- and multi-excitonic state. This coupling is hidden in the electronic Hamiltonian matrix in the representation of diabatic states (diabats) that are characterized by the excitations on the chromophore units and the linker and charge transfer among them. The seven most relevant diabats to **3**’s iSF have their leading configurations shown in Figure 2. The diabats are mainly distributed in



taking the ground state energy as 0 meV for the diagonal elements. The full matrix in 13 diabats are given in Eq. S4. The diabats' relevance to iSF is judged based on their energy gaps from and couplings with  $TGT$ ,  $EGG$ , and  $GGE$ . The direct  $EGG/GGE-TGT$  coupling is only 1 meV. This is reasonable as the  $\langle TTG | \hat{H} | EGG \rangle$  matrix element is proportional to 2-electron integrals of the frontier orbitals on the far apart **1** units.<sup>1,2</sup> The  $EGG/GGE-TGT$  coupling, if there is any, must be mediated by other diabats. Since all the other diabats are about 1 eV higher in energy than  $TGT$  and  $EGG/GGE$ , only the off-diagonal matrix elements involving one of the three and  $> 100$  meV matter. Tracking those large elements in Eq. 1, we expect the coupling pathways to be  $EGG \rightarrow CRG \rightarrow CGA/AGC \rightarrow TGT$  and its symmetry-partner  $GGE \rightarrow GCR \rightarrow AGC/CGA \rightarrow TGT$ . This is confirmed by the dynamics simulation using the electronic Hamiltonian (Figure S5). In below the discussion is focused on the first pathway.

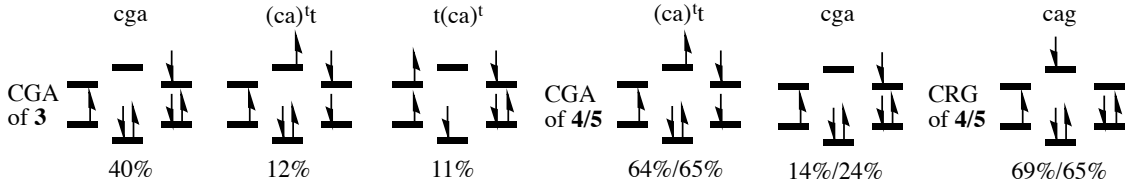


Figure 3: The compositions of some diabats. Only configurations with more than 10% contributions are shown. In the second row, the slash separates the configuration percentages in **4** and **5**.

The leading configurations in Figure 2 and the one-electron hoppings that connect them indicate that  $EGG$  is coupled to the  $cag$  and  $acg$  configurations of  $CRG$  through the respective Fock matrix elements  $F_{LC_1LLK}$  and  $F_{HC_1HLK}$ , where the subscript  $H_{LK}$  denotes the HOMO of the linker, etc. The  $cag$  configuration is coupled with  $CGA$  through  $F_{LLKLC_2}$  and  $acg$  coupled with  $AGC$  through  $F_{HLKHC_2}$ . We need to look into the compositions of  $CGA$  and  $AGC$  to understand their couplings with  $TGT$ .  $CGA$  contains 40%  $cga$ , 12%  $(ca)^t$  and 11%  $t(ca)^t$  (Figure 3). The superscript “ $t$ ” indicates the triplet character of the charge-transfer configuration among the linker and one **1** unit.  $(ca)^t$  and  $t(ca)^t$  are coupled with  $cga$  through  $F_{LLKHC_2}$  and  $F_{LC_1HLK}$ , respectively. They are also coupled with  $tgt$  through

$F_{LC_1LLK}$  and  $F_{HLKHC_2}$ .  $AGC$  and  $TGT$  are similarly coupled. This  $EGG$ -to- $TGT$  coupling pathway is schematically shown in Figure 4(a), in which each black full arrow represents a one-electron hopping driven by the corresponding Fock matrix element. Note that the triplet-pair character emerges early at the  $(ca)^{tt}$  and  $t(ca)^t$  configurations, before reaching the  $TGT$  destination. It indicates the delocalization of the triplet-pair into the linker. This delocalization is manifested by the composition of  $\mathbf{3}$ 's  $S_1^d$ :  $tgt$  contributes about 90% and the rest mainly stem from  $(ca)^{tt}$  and  $t(ca)^t$ .  $\mathbf{3}$ 's  $Q_1^d$  has a similar composition but with the corresponding quintet configurations.

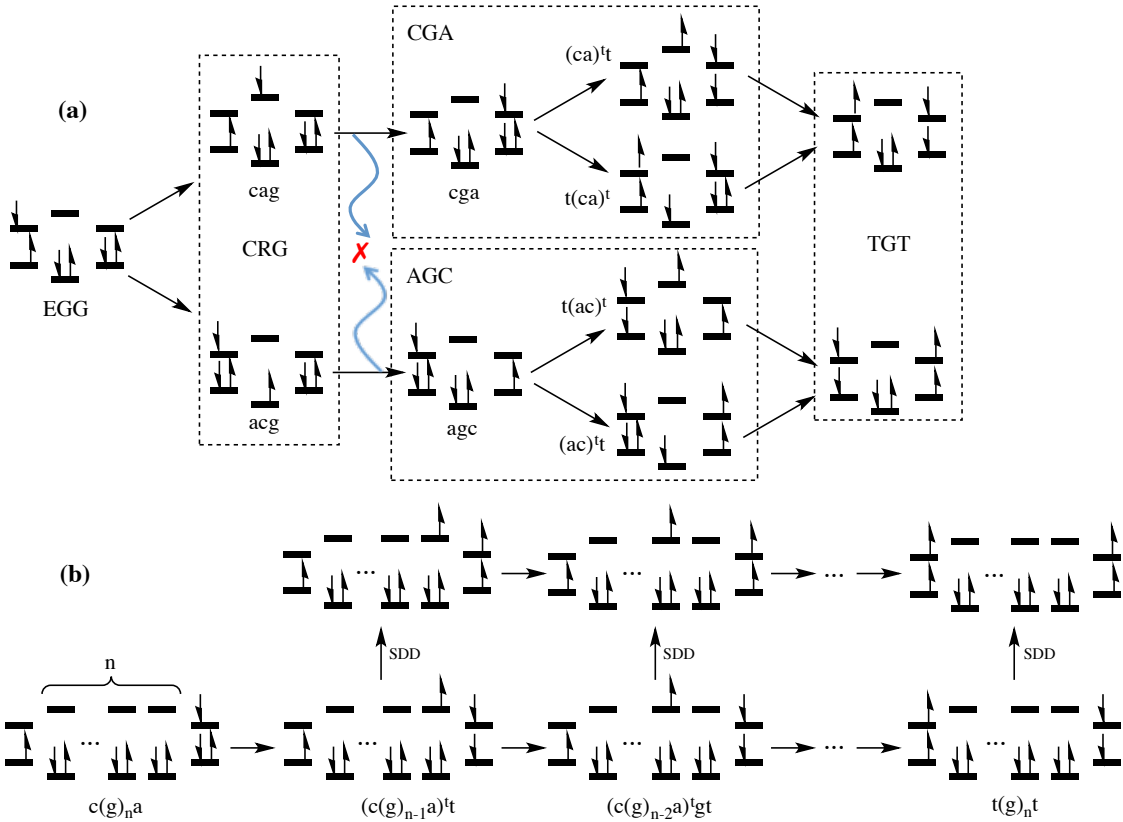


Figure 4: (a)  $\mathbf{3}$ 's electronic coupling pathway from  $EGG$  to  $TGT$ . The curvy arrows and the cross indicate the destructive interference of the upper and lower branches; (b) spin-disentanglement of the triplet-pair during electron hopping across the bridge with  $n$  linkers.

The conventional 4o4e through-space/through-contact SF picture considers two chromophore units and is well described with 5 diabats,  $TT$ ,  $EG$ ,  $GE$ ,  $CA$ , and  $AC$ , following the present naming convention.<sup>1,2</sup> The triplet-pair character is all contained in  $TT$ . The mediated

coupling pathway between single- and multi-excitonic states is  $EG/GE \rightarrow CA/AC \rightarrow TT$ . The through-linker SF picture in Figure 4(a) significantly differs from this conventional one. The larger number of mediating diabats and electronic configurations, the longer mediating pathways, and the delocalized triplet-pair manifest the through-linker effects in iSF. The triplet-pair delocalization suggests that the spin-disentanglement can occur before the triplets reach the chromophore units. As more linkers are inserted, more configurations like  $(ca)^t t$  and  $t(ca)^t$ , e.g.,  $(c(g)_{n-1}a)^t t$  and  $(c(g)_{n-2}a)^t g t$  in Figure 4(b), will participate in the electron-hopping relay between  $c(g)_n a$  and  $t(g)_n t$  ( $n$ : the number of linkers), and it will take a longer time to finish the relay. But the time is not wasted; spin-disentanglement occurs meanwhile (Figure 4(b)). This explains why two disentangled triplets are immediately formed in the iSF of BP2 (6,13-bis(triisopropylsilylethynyl)-pentacene dimer connected by 2 *para*-phenylene), vs the spin-coupled triplets in BP0 and BP1.<sup>16</sup>

Despite the intrinsically different pictures of through-linker and through-space/through-contact iSFs, one may project the former problem back to the conventional 4o4e space.<sup>44</sup> A description of the coupling pathway in Figure 4(a) using such a perturbative treatment is given in Section S4. In short, the linker’s orbitals are treated as virtual states that mediate couplings between frontier orbitals of the chromophore units. If one is interested in the linker’s (linkers’) role in spin-disentanglement, it will be more appropriate to treat the linker (linkers) explicitly. Similar to the 4o4e picture for through-space/through-contact SF, the 6o6e picture gives the most concise description for through-linker iSF that facilitates discussion of similar processes. It is of general value regardless of chromophore’s size since it has considered the most relevant frontier orbitals and electronic configurations. E.g., the similar electronic configurations and coupling pathways are expected to be in place in the iSFs of the *ortho*-bis(5-ethynyltetracenyl) benzene<sup>18</sup> and BP1.<sup>16</sup> The significance of the different configurations and branches in the pathway differs case by case. As demonstrated below, looking into the details of the coupling pathway guides us to propose chromophores with improved iSF efficiency. If the chromophore units have spatial overlap, there is also

through-space iSF arising from the  $EGG \rightarrow CGA/AGC \rightarrow TGT$  pathway and its symmetry counterpart. This is just the 6o6e analogue of the 4o4e picture, with the linker always in  $G$ .

The iSF time scale of **3** is estimated through an MCTDH simulation. The selection of vibrational modes in the vibronic model is detailed in Section S3. In brief, the modes that have large Huang-Rhys factors in **1**'s  $S_1$  and  $T_1$  excitations, and **1** and benzene's ionizations are included to describe the structural relaxation of the relevant diabats. The two torsional modes that change  $\theta$  are also included, as they modulate the frontier orbital overlaps. There are 10  $a$ - and 6  $b$ -modes (modes of the respective irreducible representations (irrep)) in the vibronic model. All 13 diabats are included in the simulation, including  $GGG$ , whose population indicates the decay to the ground state, which is not observed in all three cases below for 20 ps simulation time. A set of symmetry-adapted diabats are used in the dynamics simulation. The diabats of  $b$  irrep are taken as the  $b$  adiabats at **3**'s ground state structure, so that the initial diabat ( $EGGb'$ ) is the lowest bright diabat; the transition dipole moments of the two **1** units accumulate (cancel) in  $b$  ( $a$ ) combination. The  $a$  diabats are taken as the  $a$  adiabats at **3**'s  $Q_1^d$  structure. The so-obtained  $TGTa'$  approximates the  $S_1^d$  state at its optimized structure and makes a good target state for iSF. The name  $EGGb'$  indicates that the  $b$ -symmetry-adapted combination of  $EGG$  and  $GGE$  makes the largest contribution in this diabat, with the prime reminding us of other diabats' contributions. The other symmetry-adapted diabats are named similarly, e.g.,  $CGAa'$ ,  $GGGa'$ , etc.

The initial wave packet is the ground state vibrational wave function at the  $EGGb'$  state, representing a Franck-Condon excitation. The evolution of the state populations is shown in Figure 5(a). It takes 12 ps to plateau the  $TGTa'$  population at 70%. This time scale is commensurate with the 20 ps iSF of BP1.<sup>16</sup> The linker insertion turns off direct interaction between the chromophore units and elongates the mediated coupling pathway. It inevitably slows down the SF from having the sub-ps for directly connected dimers,<sup>16,29</sup> in exchange for the slower recombination of the triplet excitons. This statement does not contradict the reported 0.5 ps iSF of the pentacene dimer connected by *ortho*-diethynylphenyl.<sup>15</sup> It contains

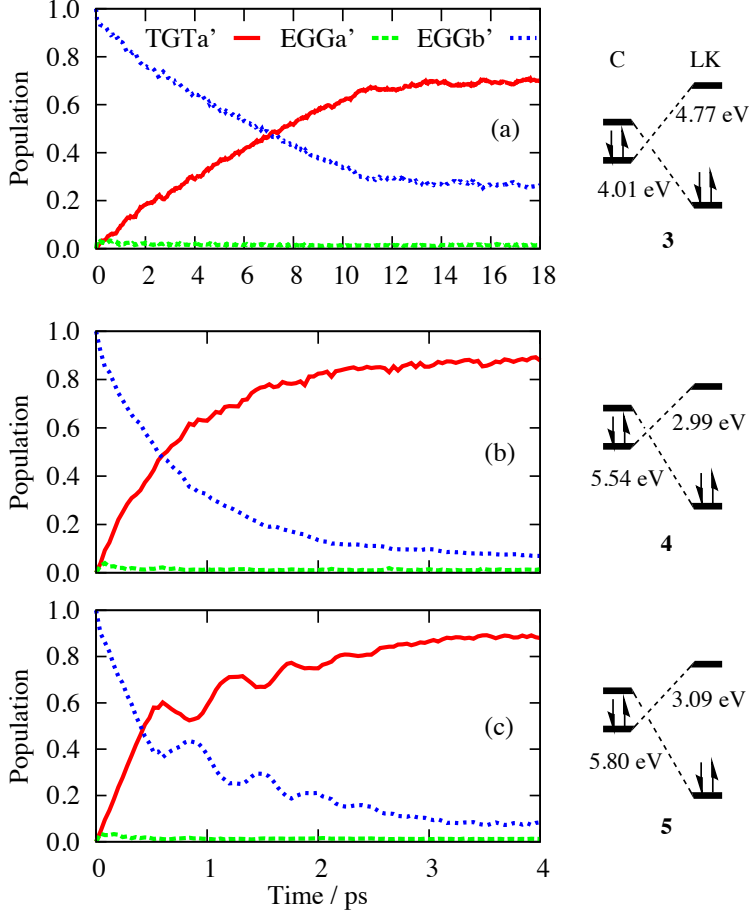


Figure 5: MCTDH simulated population evolution of (a) **3**, (b) **4**, and (c) **5**. Only the three diabats with non-negligible populations are shown. On the right of each population panel are the relative orbital energy levels for the corresponding designed molecule. The number beside each dashed line is the energy gap between the two connected orbital levels.

through-space effects<sup>44</sup> that are deliberately avoided here. Other than the initial and final states, only  $EGGa'$  is non-negligibly populated in the early time. It then loses its population as the  $TGTa'$  population increases. Bearing the similar single-excitonic character,  $EGGb'$  first transfers its population to  $EGGa'$  through the  $b$  coupling modes. The  $EGGa'$  population is subsequently passed to the more stable  $TGTa'$  through their electronic coupling and  $a$ -mode-driven vibronic coupling. The mediating configurations in Figure 4(a) contribute to  $EGGa'$  and  $TGTa'$  and hence participate in the population transfer.

The 12 ps time scale is fairly short for through-linker iSF. It outcompetes fluorescence and intersystem crossing, which are usually of ns and ms time scales, respectively. However, it is

interesting to further enhance the iSF rate through modulating the linker. Given the many deactivation channels for the single-excitonic state when a chromophore is immersed in a real environment,<sup>1</sup> a faster iSF is always sought.  $\langle CGA | \hat{H} | CRG \rangle$  and  $\langle AGC | \hat{H} | CRG \rangle$  in Eq. 1 are of similar magnitude, 283 vs 201 meV. The linear combination of  $CGA$  and  $AGC$  that transforms following the  $a$  irrep reads  $|CGAa\rangle = \sqrt{\frac{1}{2}}(|CGA\rangle - |AGC\rangle)$ . Therefore, the two fairly large matrix elements cancel and result in  $\langle CGAa | \hat{H} | CRG \rangle = 58$  meV. As  $TGT$  is of  $a$  irrep and coupled to  $CGAa$ , not  $CGAb$ , the cancellation leads to a destructive interference of the two branches of the pathway shown in Figure 4(a). Making the two matrix elements more different should improve the iSF rate. Note that while the pathway in Figure 4(a) is general, this interference is specific for **3**.

The almost equivalent  $cag$  and  $acg$  contributions in  $CRG$  are responsible for the the two similar matrix elements, as they are respectively coupled to  $CGA$  and  $AGC$  (see above and Section S4). If we shift down the energies of  $H_{LK}$  and  $L_{LK}$ , it will be easier to transfer an electron from  $H_{C1}$  to  $L_{LK}$  to form  $cag$ , than transfer from  $H_{LK}$  to  $L_{C1}$  to form  $acg$ . The equivalence of their contributions will be broken and the destructive interference will be alleviated. We then construct a model molecule **4** with four Cl atoms on the linker. The Cl atoms are bulky enough to give a  $51^\circ$   $\theta$  in **4**'s  $S_1^d$ -optimized structure. The close-to-1 (Figure S1) occupancies of HONO-1 to LUNO+1 in  $S_1^d$  indicate the state's tetraradical nature. The minimum-to-minimum  $S_1^d$ - $Q_1^d$  is only 0.09 eV, significantly smaller than the 0.63 eV iSF exoergicity. The electronegative Cl atoms do shift down the  $H_{LK}$  and  $L_{LK}$  energies. The  $H_{C1}$ - $L_{LK}$  gap changes from 4.77 to 2.99 eV and the  $H_{LK}$ - $L_{C1}$  gap from 4.01 to 5.54 eV (Figure 5). Consequently, **4**'s  $CRG$  contains 69%  $cag$  and no  $acg$  (Figure 3). For the ease of forming the anionic linker, the  $CRG$  energy is shifted down to be only 349 meV higher than  $EGG$  (Eq. S5); it is more active in bridging the coupling pathway.  $\langle CGA | \hat{H} | CRG \rangle$  and  $\langle AGC | \hat{H} | CRG \rangle$  become 329 and  $-26$  meV; the  $cag$  branch in Figure 4(a) dominates and there is no destructive interference.

The ease of forming the anionic linker also increases the  $(ca)^t t$  contribution in  $CGA$  to

64%, and hence increases  $\langle TGT | \hat{H} | CGA \rangle$  to 351 meV. Despite its only 14% *cga* contribution, we still call the diabat *CGA* since it is obtained following the same maximization of its *cga* character as in **3**. The stronger mediated *EGG-TGT* coupling is confirmed by the electronic dynamics shown in Figure S6(a). **4**'s iSF is completed within 3 ps, 4 times faster than in **3**, and reaches a larger eventual *TGT* population, 90% (Figure 5(b)). To our knowledge, no faster through-linker iSF has ever been reported, in experimental or theoretical works. The strategy of tuning the iSF rate through modulating the linker works as planned.

The presence of four Cl atoms in **4** raises a concern of the possible efficient intersystem crossing (ISC) that may be faster than iSF.<sup>45</sup> The ISC may convert the singlet single-excitonic state to a triplet single-excitonic state, which does not have enough energy to undergo iSF. The spin-orbit (SO) couplings between **4**'s *EGGb'* and the nearby triplet single excitonic  $T_{1,2,4}^d$  are evaluated to have the magnitudes 0.52, 1.03, and 1.01  $\text{cm}^{-1}$ . The triplets are 1.42 and 1.45 eV lower and 0.35 eV higher than *EGGb'*, respectively, and the time scale for ISCs from *EGGb'* to them are evaluated (Section S5) to be  $\sim 10^{-4} - 10^{-5}$  s. The ISCs are hence not competitive with the ps-fast iSF, not even if the SO couplings were enlarged 100 times and the ISC time scales were shortened to  $\sim$  ns.

Despite the unlikelihood of the detrimental ISC in **4**, we propose **5** to replace the Cl atoms by F. A methyl is introduced to an N of the **1** unit to maintain  $\theta = 53^\circ$  in its  $S_1^d$  and prevent large  $S_1^d$ - $Q_1^d$  gap. The tetradical character is evidenced by its natural orbital occupancies (Figure S1). **5**'s 0.12 eV minimum-to-minimum  $S_1^d$ - $Q_1^d$  gap is smaller than its 0.47 eV iSF exoergicity. Similar orbital energy down-shifts are seen (Figure 5); *CRG* and *CGA* are again dominated by *cag* and  $(ca)^{tt}$  (Figure 3). Similar changes of Hamiltonian matrix elements (Eq. S6) as in **4** are seen in **5**, except for **5**'s higher *CRG* energy, 738 meV above *EGG*. The *CRG* is then less active in bridging the coupling pathway, as shown by the comparison of Figure S6(a) and (b). The more diffuse Cl atoms make the linker easier to form an anion and lower the *CRG* energy. This trend is consistent with the more negative electron affinity of Cl than F ( $-3.6$  vs  $-3.4$  eV).<sup>46,47</sup> **5**'s *TGTa'* population rises to 90%

within 4 ps (Figure 5(c)), only slightly slower than in **4**. The success of **5** indicates that the H on the N atoms can be replaced by an alkyl group. This greatly enhances the diversity in derivative chromophores based on **3** – **5**. Also, the **1** with both N atoms methylated is isoelectronic and isosteric to **1'**, a SF chromophore designed by Michl et al.<sup>25</sup> The **3** – **5** analogues with the **1** unit being replaced by **1'** are likely to be promising iSF chromophores. This further enhances the chromophore diversity beyond the realm of azaborine chemistry.

BP1 features the same linker and has been thoroughly investigated by Sanders et al.<sup>16,30</sup> They have also studied the tetrafluorophenylene analogue of BP1, whose iSF is slowed down to 80 ps.<sup>48</sup> This slowdown does not contradict the speedup in **5** vs **3**. Our geometry optimizations show that BP1 and the tetrafluoro-BP1 have 36° and 41° for their  $\theta$  analogues. The relevant Fock matrix elements should be slightly reduced in magnitude by the F atoms. Also, if *CRG* of BP1 contains more *cag* than *acg*, the fluorination may equilibrate their contributions and a more destructive interference ensues.

In summary, we investigate the through-linker mechanism of through-linker intramolecular singlet fission (iSF) using the *para*-phenylene linker and the diazadiborine chromophore (**1**) as the model. The electronic coupling pathway from the single- to the multi-excitonic state is elucidated. Charge-transfer states with an ionic linker are the key steps to connect the two types of excitonic states. The triplet-pair character is delocalized into the linker and hidden in some charge-transfer configurations (e.g.,  $(ca)^{tt}$ ). This 6o6e through-linker iSF picture is the first time presented. It clearly displays the difference from the conventional 4o4e picture for through-space/through-contact singlet fission. It is of general value since it has covered all key frontier orbitals of chromophores and linker and the energy-most-accessible electronic states. What differ case by case are the coupling strengths of the configurations, modulation of their energies, and the presence/absence of some interference between coupling channels. Guided by the 6o6e picture, we propose to chlorinate and fluorinate the linker of **3** to alleviate the destructive interference in its coupling pathway, resulting in **4** and **5** with faster iSFs. The ps-fast iSFs in **3** – **5** make them and their derivatives high-value targets for

azaborine synthesis.

## ASSOCIATED CONTENT

**Supporting information** The supporting information is available free of charge *via* the Internet at <http://pubs.acs.org>.

More details of computational methods; the  $S_1^d$  natural orbitals of **3** – **5**; compositions of the 13 diabats of **3** – **5**; electronic Hamiltonian matrices in all 13 local diabats of **3** – **5**; selection of vibrational modes in MCTDH simulations; perturbative description of **3**'s *EGG-TGT* coupling pathway; discussion of the ISC time scale in **4**; coordinates of discussed structures.

## NOTE

The authors declare no competing financial interest.

## ACKNOWLEDGEMENTS

Computations were made on the supercomputer Mammoth parallelèl 2 from Université de Sherbrooke, managed by Calcul Québec and Compute Canada. We thank Carleton University for the start-up grant (186853) and the Natural Sciences and Engineering Research Council (NSERC) of Canada for funding (RGPIN-2016-06276). We thank Josef Michl (University of Colorado Boulder) and Samuel Sanders (Columbia University) for enlightening discussion. We are grateful to Mike Schmidt and Mark Gordon (Iowa State University) for their continuous support of the GAMESS-US program package. We also thank Hans-Dieter Meyer (Universität Heidelberg) for his generosity of providing us with the MCTHD package.

## References

- (1) Smith, M. B.; Michl, J. Singlet Fission. *Chem. Rev.* **2010**, *110*, 6891–6936.
- (2) Smith, M. B.; Michl, J. Recent Advances in Singlet Fission. *Annu. Rev. Phys. Chem.* **2013**, *64*, 361–386.
- (3) Shockley, W.; Queisser, H. J. Detailed Balance Limit of Efficiency of P-N Junction Solar Cells. *J. Appl. Phys.* **1961**, *32*, 510–519.
- (4) Hanna, M. C.; Nozik, A. J. Solar Conversion Efficiency of Photovoltaic and Photoelectrolysis Cells with Carrier Multiplication Absorbers. *J. Appl. Phys.* **2006**, *100*, 074510.
- (5) Johnson, J. C.; Nozik, A. J.; Michl, J. The Role of Chromophore Coupling in Singlet Fission. *Acc. Chem. Res.* **2013**, *46*, 1290–1299.
- (6) Piland, G. B.; Bardeen, C. J. How Morphology Affects Singlet Fission in Crystalline Tetracene. *J. Phys. Chem. Lett.* **2015**, *6*, 1841–1846.
- (7) Pensack, R. D.; Tilley, A. J.; Parkin, S. R.; Lee, T. S.; Payne, M. M.; Gao, D.; Jahnke, A. A.; Oblinsky, D. G.; Li, P.-F.; Anthony, J. E. et al. Exciton Delocalization Drives Rapid Singlet Fission in Nanoparticles of Acene Derivatives. *J. Am. Chem. Soc.* **2015**, *137*, 6790–6803.
- (8) Tamura, H.; Huix-Rotllant, M.; Burghardt, I.; Olivier, Y.; Beljonne, D. First-Principles Quantum Dynamics of Singlet Fission: Coherent Versus Thermally Activated Mechanisms Governed by Molecular  $\pi$  Stacking. *Phys. Rev. Lett.* **2015**, *115*, 107401.
- (9) Müller, A. M.; Avlasevich, Y. S.; Müllen, K.; Bardeen, C. J. Evidence for Exciton Fission and Fusion in a Covalently Linked Tetracene Dimer. *Chem. Phys. Lett.* **2006**, *421*, 518–522.

- (10) Johnson, J. C.; Akdag, A.; Zamadar, M.; Chen, X.; Schwerin, A. F.; Paci, I.; Smith, M. B.; Havlas, Z.; Miller, J. R.; Ratner, M. A. et al. Toward Designed Singlet Fission: Solution Photophysics of Two Indirectly Coupled Covalent Dimers of 1,3-Diphenylisobenzofuran. *J. Phys. Chem. B* **2013**, *117*, 4680–4695.
- (11) Monahan, N.; Zhu, X.-Y. Charge Transfer-Mediated Singlet Fission. *Annu. Rev. Phys. Chem.* **2015**, *66*, 601–618.
- (12) Cook, J. D.; Carey, T. J.; Damrauer, N. H. Solution-Phase Singlet Fission in a Structurally Well-Defined Norbornyl-Bridged Tetracene Dimer. *J. Phys. Chem. A* **2016**, *120*, 4473–4481.
- (13) Busby, E.; Xia, J.; Wu, Q.; Low, J. Z.; Song, R.; Miller, J. R.; Zhu, X.-Y.; Campos, L. M.; Sfeir, M. Y. A Design Strategy for Intramolecular Singlet Fission Mediated by Charge-Transfer States in Donor–Acceptor Organic Materials. *Nature Mater.* **2015**, *14*, 426–433.
- (14) Trinh, M. T.; Zhong, Y.; Shen, Q.; Schiros, T.; Jockusch, S.; Sfeir, M. Y.; Steigerwald, M.; Nuckolls, C.; Zhu, X.-Y. Intra- to Intermolecular Singlet Fission. *J. Phys. Chem. C* **2015**, *119*, 1312–1319.
- (15) Zirzmeier, J.; Lehnerr, D.; Coto, P. B.; Chernick, E. T.; Casillas, R.; Basel, B. S.; Thoss, M.; Tykwinski, R. R.; Guldi, D. M. Singlet Fission in Pentacene Dimers. *Proc. Natl. Acad. Sci. USA* **2015**, *112*, 5325–5330.
- (16) Sanders, S. N.; Kumarasamy, E.; Pun, A. B.; Trinh, M. T.; Choi, B.; Xia, J.; Taffet, E. J.; Low, J. Z.; Miller, J. R.; Roy, X. et al. Quantitative Intramolecular Singlet Fission in Bipentacene. *J. Am. Chem. Soc.* **2015**, *137*, 8965–8972.
- (17) Lukman, S.; Musser, A. J.; Chen, K.; Athanasopoulos, S.; Yong, C. K.; Zeng, Z.; Ye, Q.; Chi, C.; Hodgkiss, J. M.; Wu, J. et al. Tuneable Singlet Exciton Fission and Triplet-

- Triplet Annihilation in an Orthogonal Pentacene Dimer. *Adv. Funct. Mater.* **2015**, *25*, 5452–5461.
- (18) Korovina, N. V.; Das, S.; Nett, Z.; Feng, X.; Joy, J.; Haiges, R.; Krylov, A. I.; Bradforth, S. E.; Thompson, M. E. Singlet Fission in a Covalently Linked Cofacial Alkynyl-tetracene Dimer. *J. Am. Chem. Soc.* **2016**, *138*, 617–627.
- (19) Low, J. Z.; Sanders, S. N.; Campos, L. M. Correlating Structure and Function in Organic Electronics: from Single Molecule Transport to Singlet Fission. *Chem. Mater.* **2015**, *27*, 5453–5463.
- (20) Minami, T.; Nakano, M. Diradical Character View of Singlet Fission. *J. Phys. Chem. Lett.* **2012**, *3*, 145–150.
- (21) Scholes, G. D. Correlated Pair States Formed by Singlet Fission and Exciton–Exciton Annihilation. *J. Phys. Chem. A* **2015**, *119*, 12699–12705.
- (22) Feng, X.; Krylov, A. I. On Couplings and Excimers: Lessons from Studies of Singlet Fission in Covalently Linked Tetracene Dimers. *Phys. Chem. Chem. Phys.* **2016**, *18*, 7751–7761.
- (23) Paci, I.; Johnson, J. C.; Chen, X. D.; Rana, G.; Popović, D.; David, D. E.; Nozik, A. J.; Ratner, M. A.; Michl, J. Singlet Fission for Dye-Sensitized Solar Cells: Can a Suitable Sensitizer be Found? *J. Am. Chem. Soc.* **2006**, *128*, 16546–16553.
- (24) Johnson, J. C.; Nozik, A.; Michl, J. High Triplet Yield from Singlet Fission in a Thin Film of 1,3-Diphenylisobenzofuran. *J. Am. Chem. Soc.* **2010**, *132*, 16302–16303.
- (25) Akdag, A.; Havlas, Z.; Michl, J. Search for a Small Chromophore with Efficient Singlet Fission: Biradicaloid Heterocycles. *J. Am. Chem. Soc.* **2012**, *134*, 14624–14631.
- (26) Zeng, T.; Ananth, N.; Hoffmann, R. Seeking Small Molecules for Singlet Fission: a Heteroatom Substitution Strategy. *J. Am. Chem. Soc.* **2014**, *136*, 12638–12647.

- (27) Wen, J.; Havlas, Z.; Michl, J. Captodatively Stabilized Biradicaloids as Chromophores for Singlet Fission. *J. Am. Chem. Soc.* **2015**, *137*, 165–172.
- (28) Bhattacharyya, K.; Pratik, S. M.; Datta, A. Small Organic Molecules for Efficient Singlet Fission: Role of Silicon Substitution. *J. Phys. Chem. C* **2015**, *119*, 25696–25702.
- (29) Zeng, T.; Goel, P. Design of Small Intramolecular Singlet Fission Chromophores: An Azaborine Candidate and General Small Size Effects. *J. Phys. Chem. Lett.* **2016**, *7*, 1351–1358.
- (30) Sanders, S. N.; Kumarasamy, E.; Pun, A. B.; Appavoo, K.; Steigerwald, M. L.; Campos, L. M.; Sfeir, M. Y. Exciton Correlations in Intramolecular Singlet Fission. *J. Am. Chem. Soc.* **2016**, *138*, 7289–7297.
- (31) Zhao, Y.; Truhlar, D. G. The M06 Suite of Density Functionals for Main Group Thermochemistry, Thermochemical Kinetics, Noncovalent Interactions, Excited States, and Transition Elements: Two New Functionals and Systematic Testing of Four M06-Class Functionals and 12 Other Functionals. *Theoret. Chem. Acc.* **2008**, *120*, 215–241.
- (32) Nakano, H.; Uchiyama, R.; Hirao, K. Quasi-Degenerate Perturbation Theory with General Multiconfiguration Self-Consistent Field Reference Functions. *J. Comput. Chem.* **2002**, *23*, 1166–1175.
- (33) Li, S. L.; Truhlar, D. G.; Schmidt, M. W.; Gordon, M. S. Model Space Diabatization for Quantum Photochemistry. *J. Chem. Phys.* **2015**, *142*, 064106.
- (34) Atchity, G. J.; Ruedenberg, K. Orbital Transformations and Configurational Transformations of Electronic Wavefunctions. *J. Chem. Phys.* **1999**, *111*, 2910–2920.
- (35) Dunning, T. H. Gaussian Basis Sets for Use in Correlated Molecular Calculations. I. The Atoms Boron Through Neon and Hydrogen. *J. Chem. Phys.* **1989**, *90*, 1007–1023.

- (36) Sakai, Y.; Miyoshi, E.; Klobukowski, M.; Huzinaga, S. Model Potentials for Main Group Elements Li through Rn. *J. Chem. Phys.* **1997**, *106*, 8084–8092.
- (37) Schmidt, M. W.; Baldrige, K. K.; Boatz, J. A.; Elbert, S. T.; Gordon, M. S.; Jensen, J. H.; Koseki, S.; Matsunaga, N.; Nguyen, K. A.; Su, S. et al. General Atomic and Molecular Electronic Structure System. *J. Comput. Chem.* **1993**, *14*, 1347–1363.
- (38) Gordon, M. S.; Schmidt, M. W. In *Theory and Applications of Computational Chemistry: The First Forty Years*; Dykstra, C. E., Frenking, G., Kim, K. S., Scuseria, G. E., Eds.; Elsevier: Amsterdam, 2005.
- (39) Beck, M. H.; Jäckle, A.; Worth, G. A.; Meyer, H.-D. The Multiconfiguration Time-Dependent Hartree Method: A Highly Efficient Algorithm for Propagating Wavepackets. *Phys. Rep.* **2000**, *324*, 1–105.
- (40) Campbell, P. G.; Marwitz, A. J. V.; Liu, S.-Y. Recent Advances in Azaborine Chemistry. *Angew. Chem. Int. Ed.* **2012**, *51*, 6074–6092.
- (41) Braunschweig, H.; Geetharani, K.; Jimenez-Halla, J. O. C.; Schäfer, M. Direct Synthetic Route to Functionalized 1,2-Azaborines. *Angew. Chem. Int. Ed.* **2014**, *126*, 3568–3572.
- (42) Casanova, J.; Kiefer, H. R.; Kuwada, D.; Boulton, A. H. 1,3-Diaza-2,4-Diboretidines. Isocyanide-Borane Adducts. 11. *Tetrahedron Lett.* **1965**, *6*, 703–714.
- (43) Forster, T. D.; Krahulic, K. E.; Tuononen, H. M.; McDonald, R.; Parvez, M.; Roesler, R. A  $\sigma$ -Donor with a Planar Six- $\pi$ -Electron B<sub>2</sub>N<sub>2</sub>C<sub>2</sub> Framework: Anionic N-Heterocyclic Carbene or Heterocyclic Terphenyl Anion? *Angew. Chem. Int. Ed.* **2006**, *45*, 6356–6359.
- (44) Ito, S.; Nagami, T.; Nakano, M. Design Principles of Electronic Couplings for Intramolecular Singlet Fission in Covalently-Linked Systems. *J. Phys. Chem. A* **2016**, *120*, 6236–6241.

- (45) Klessinger, M.; Michl, J. *Excited States and Photochemistry of Organic Molecules*; VCH Publishers, Inc.: New York, 1995.
- (46) Berzinsh, U.; Gustafsson, M.; Hanstorp, D.; Klinkmüller, A.; Ljungblad, U.; Martensson-Pendrill, A. M. Isotope Shift in the Electron Affinity of Chlorine. *Phys. Rev. A* **1995**, *51*, 231–238.
- (47) Blondel, C.; Delsart, C.; Goldfarb, F. Electron Spectrometry at the  $\mu\text{eV}$  Level and the Electron Affinities of Si and F. *J. Phys. B* **2001**, *34*, L281–L288.
- (48) Sanders, S. *Private communication*